

Hot Corrosion Behaviour of HVOF Sprayed (Cr_3C_2 -35 % NiCr) + 5 % Si Coatings in the Presence of Na_2SO_4 -60 % V_2O_5 at 700 °C

B. Somasundaram · Ravikiran Kadoli ·
M. R. Ramesh

Received: 12 April 2014 / Accepted: 4 August 2014 / Published online: 26 October 2014
© The Indian Institute of Metals - IIM 2014

Abstract The hot corrosion behavior of high velocity oxyfuel sprayed (Cr_3C_2 -35 % NiCr) + 5 % Si coatings on three substrate alloys of SA213-T22, MDN-310 and Superfer 800 H was investigated. The as-sprayed coatings are characterized with respect to microstructure and mechanical properties. Thermocyclic hot corrosion studies were performed in a molten salt environment of Na_2SO_4 -60 % V_2O_5 for 50 cycles at 700 °C. Thermogravimetric technique was used to establish the kinetics of hot corrosion of uncoated and coated steels. It was observed that the coated steel showed better hot corrosion resistance than the uncoated steels. The coated steels follow the parabolic rate law of oxidation and the parabolic rate constant values are appreciably lower in comparison to the uncoated steels. The coated steels showed slow oxidation kinetics which indicated that the reaction rate is diffusion limited. The oxides of Cr_2O_3 and SiO_2 formed on the outermost surface of the coatings are found to be passive in the molten NaVO_3 melt.

Keywords HVOF · Thermal spray process · Cr_3C_2 -NiCr · Hot corrosion · Surface analysis · Thermal cycling

1 Introduction

Fire side corrosion and erosion of metallic structural materials at elevated temperature in complex multicomponent gas environments that include particulates are potential problems in many fossil energy systems, especially those using coal as a feedstock [1]. In addition future trends may actually increase the occurrence of fireside corrosion. For example, an increase in the steam temperature to raise the thermal efficiency, the widening use of lower rank coals with larger percentages of impurities, shortage of metals used to make corrosion resistant alloys and the imposition of more emission and other environmental controls could all adversely affect the corrosion behavior of the system [2].

Power plants are one of the major industries distressed from severe corrosion problems resulting in the significant losses. For instance, steam temperature of boilers is limited by corrosion and creep resistance of boiler components, which affects the thermal efficiency of the boilers. Consequently, the thermal efficiency decreases and hence the electricity production is reduced [3]. High temperature corrosion and erosion of heat exchange tubes and other structural materials in coal-fired boilers are recognized as being the main cause of downtime at power-generating plants, which could account for 50–75 % of their total arrest time. Maintenance costs for replacing broken tubes in some of these installations are also very high, and can be estimated at up to 54 % of the total production costs [4].

The existing structural materials used in coal-fired plants are fabricated from low-alloy carbon steels with chromium and molybdenum as the principal alloying elements. Although chromium is expected to impart corrosion resistance, its concentration in the boiler tube alloys is not sufficient to form a protective oxide layer [2]. A potential

B. Somasundaram
Department of Mechanical Engineering, Reva Institute of
Technology and Management, Yelahanka, Bangalore 560 064,
India

R. Kadoli · M. R. Ramesh (✉)
Department of Mechanical Engineering, National Institute of
Technology Karnataka, Surathkal, Mangalore 575 025, India
e-mail: rameshmr@nitk.edu.in

approach to handle with these problems is by using corrosion resistant coatings with good thermal conductivities [4]. The role of the coatings is to provide a metal surface composition that will react with the environment to produce the most protective scale possible, which can inhibit corrosion along with long term stability and providing resistance to cracking or spallation under severe mechanical and thermal stresses [5].

The HVOF process is a relatively new thermal spray process, offering coatings with higher bond strength and hardness, together with lower porosity as compared with other thermal spraying counterparts such as flame spraying, arc spraying and plasma spraying [6]. The possibilities of applying the HVOF process to a much wider range of materials are now being addressed and there are several reports in the literature relating to the spraying of Ni and other metallic alloys for corrosion resistant applications where dense, microstructurally homogeneous coatings are essential [7].

The most common HVOF cermets coatings are WC–Co, WC–CoCr, and Cr₃C₂–NiCr systems. WC–Co and WC–CoCr coatings show good tribological properties in rigorous working conditions such as at high temperatures or in aggressive environments [8, 9]. Cr₃C₂–NiCr coating is considered to be an excellent replacement for the thermal sprayed Cr₂O₃ coatings, but indicated spalling of surface oxide scale during the thermo cyclic oxidation studies in molten salt environment [10, 11]. Gurrappa [12] reported that the plasma sprayed coatings of NiCoCrAlY with Hafnium and Silicon addition improves scale adhesion and oxidation resistance. Ramesh et al. [13] and Wu and Niu [14] suggested that the critical Si concentration in the range between 4 and 6 wt% in Ni–Si based coatings is sufficient to form SiO₂ layer, which exhibit good oxidation and hot corrosion resistance. Also additions of 4.3 wt% Si reduce the oxygen contents in the coatings, especially during the in-flight period at higher particles temperature [15]. In the present work, Cr₃C₂–NiCr powder is alloyed with 5 % silicon and this composite coating produced with HVOF process has been characterized in terms of microstructures, porosity, phase composition, microhardness and bond strength. The thermo cyclic hot corrosion tests for (Cr₃C₂–35 % NiCr) + 5 % Si coated and uncoated boiler tube steels have been conducted in a molten salt environment of Na₂SO₄–60 % V₂O₅ for 50 cycles at 700 °C. The thermo

cyclic experiments constitute a more realistic approach towards solving the problem of industrial origin where conditions are more or less cyclic.

2 Experimental Procedures

2.1 Development of Coatings

2.1.1 Substrate Materials

The Fe-based Superalloy designated as Superfer 800 (Midhani Grade), chrome moly steel designated as ASTM-SA213-T22 and austenitic steel designated as MDN 310 (Midhani Grade) were used as substrate materials. These materials are employed for applications in furnace equipment, steam boilers and super heater tubes in coal-fired power plants. The chemical composition of the substrate alloys is reported in the Table 1. The specimens with approximate dimensions of 25 mm × 25 mm × 5 mm were prepared for corrosion studies, grounded using SiC abrasive papers down to 180 grit and subsequently were grit-blasted with Al₂O₃ (Grit 45) before HVOF spraying for developing better adhesion of the coating to the substrate.

2.1.2 Coating Formulation

HVOF spraying has been carried out using a HIPOJET 2700 equipment (M/S Metallizing Equipment Co. Pvt. Ltd., Jodhpur, India), which utilizes the supersonic jet generated by the combustion of liquid petroleum gas and oxygen mixture. A commercially available Cr₃C₂–NiCr powder of nominal composition [Cr–30 Ni–9.5 C] (wt%) was mechanically blended with 5 % Si was used as feed-stock alloy. As evident from the micrographs of the coating powders as shown in Fig. 1, the (Cr₃C₂–35 % NiCr) + 5 % Si powder particles have irregular shaped particles of variable shapes and sizes. The particle size distribution of the powder as determined by the image analysis of the secondary electron micrographs are found to be –45 + 15 μm, consistent with the nominal size distribution as provided by the manufacturer. Employed spraying parameters during HVOF projection are listed in Table 2. All the process parameters, including the spray distance were kept constant throughout the coating process

Table 1 Chemical composition (wt%) of boiler tube steels

Type of steel	Fe	Ni	Cr	Ti	Al	Mo	Mn	Si	C
SA213-T22	Bal.	–	2.55	–	–	1.10	0.52	0.43	0.14
MDN 310	Bal.	21	25	–	–	–	2.00	0.80	0.10
Superfer 800	Bal.	32	21.0	0.30	0.30	–	1.50	1.00	0.10

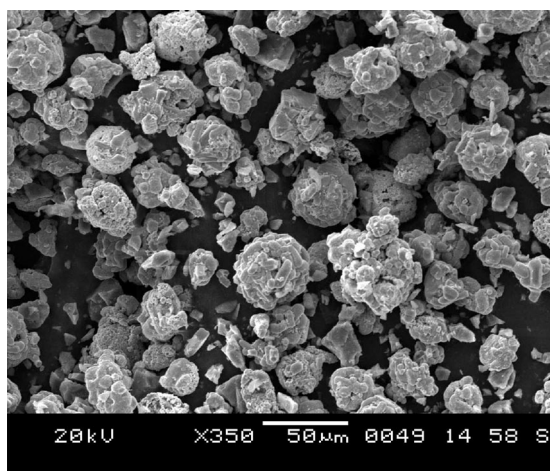


Fig. 1 Scanning electron micrograph of $(\text{Cr}_3\text{C}_2\text{-}35\% \text{ NiCr}) + 5\% \text{ Si}$ powder

Table 2 Spray parameters employed for HVOF spray process

Oxygen flow rate	250 l/min
Fuel (LPG) flow rate	65–70 l/min
Air-flow rate	550 l/min
Spray distance	178 mm
Powder feed rate	38 g/min
Fuel pressure	681 kPa
Oxygen pressure	981 kPa
Air pressure	588 kPa

and the powder was sprayed on all the faces of the substrate alloy.

2.2 Characterization Techniques

X-ray diffraction patterns (XRD) (Bruker AXS D-8 Advance Diffractometer with CuK_α radiation and nickel filter at 20 mA under a voltage of 35 kV) were obtained for feed stock powders, as-sprayed coatings and corroded products. The coating morphology and the elemental compositions were characterized using Scanning Electron Microscope (JEOL JSM-6380LA). The coating thickness was measured by obtaining a backscattered electron image (BSEI) with a scanning electron microscope which was attached to a backscattered detector. Zeiss Axiovert 200 MAT inverted optical microscope, interfaced with image analysing software was used to obtain an optical image along the cross-section of as-sprayed coatings and to determine the porosity content. Vickers micro hardness measurements (Matsuzawa MXT-50 Microhardness Tester, Japan) as per ASTM E384 standard using 300 g load were performed in order to assess the hardness of as-sprayed coatings. The bond strength of coatings was accessed in accordance with ASTM C633 standards.

2.3 Thermocyclic Corrosion

Cyclic hot corrosion studies were performed in a molten salt environment of $\text{Na}_2\text{SO}_4\text{-}60\% \text{ V}_2\text{O}_5$ for 50 cycles under cyclic conditions. Each cycle consisted of 1 h heating at 700 °C in silicon carbide tube furnace followed by 20 min cooling at room temperature. The studies were performed for uncoated as well as coated specimens for comparison. The specimens were heated in an oven to about 250 °C. The heating of the specimens was found essential for proper adhesion of the salt layer. A salt of $\text{Na}_2\text{SO}_4\text{-}60\% \text{ V}_2\text{O}_5$ is thoroughly mixed with distilled water. Thereafter, a layer of $\text{Na}_2\text{SO}_4\text{-}60\% \text{ V}_2\text{O}_5$ mixture was applied uniformly to the warm specimens with the help of a camel hair brush. The amount of the salt coating was kept in the range of 3.0–5.0 mg/cm^2 . The salt coated specimens were then kept in the alumina boats and then loaded into the oven for 3–4 h at 100 °C for drying and proper adhesion of the salt. After drying, the salt coated samples along with boat were weighed and then introduced in the silicon carbide tube furnace kept at 700 °C. During hot corrosion runs, the weight of boats and specimens was measured together at the end of each cycle with the help of an Electronic Balance Model AY-120 (Shimadzu, Kyoto, Japan) with a sensitivity of 1 mg. The samples after being subjected to corrosion were analysed using SEM/EDAX and XRD techniques.

3 Results

3.1 Characterization of As-sprayed Coating

3.1.1 Coating Thickness and Porosity

The coatings have been sprayed by moving the HVOF gun on a stationary substrate, and by varying the number of passes the desired thickness of the coatings has been achieved. The thickness of the coatings has been found to be in the range of 350–400 μm . The porosity of the coatings has a significant role to play as far as the corrosion resistance of coatings is considered. Dense coatings usually provide better oxidation and corrosion resistance than the porous coatings. The average porosity value of the coatings was found to be 1.5 %.

3.1.2 Microhardness of the Coatings

Figure 2 shows microhardness profile along the cross-section of $(\text{Cr}_3\text{C}_2\text{-}35\% \text{ NiCr}) + 5\% \text{ Si}$ coatings as a function of distance from the coating–substrate interface. As indicated by the microhardness profiles, the average values of microhardness for the $(\text{Cr}_3\text{C}_2\text{-}35\% \text{ NiCr}) + 5\% \text{ Si}$

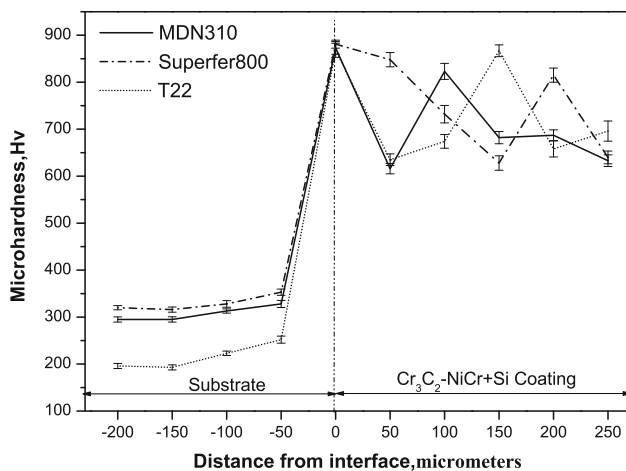


Fig. 2 Microhardness profiles of $(\text{Cr}_3\text{C}_2\text{-}35\% \text{ NiCr}) + 5\% \text{ Si}$ coated steels along the cross-section

coating is of the order of 736 Hv. The microhardness of the coatings is found to vary along the cross-section due to the distribution of the Cr_3C_2 hard phase in NiCr matrix. Furthermore, a considerable increase in the microhardness values is measured on the substrate region closer to the coating. This increased hardness is partially due to the higher kinetic energies of powder particles and partially due to the work hardening of substrate during sandblasting prior to the HVOF spraying. A similar trend of increased hardness in the substrate during the HVOF coating has been discussed by Sundararajan et al. [16].

3.1.3 Bond Strength of the Coatings

The tensile adhesive strength (bond strength) of the as-sprayed coatings was evaluated using the standardized method in accordance with ASTM C633. The test sample covered on one front side by the coating is joined with the loading and bolstering member using the suitable adhesive medium. The glue used is HTK Ultra Bond epoxy glue, with characteristic tensile strength of 80 N/mm^2 . After the thermal curing of the glued joint, the tension test was performed in bond strength tester Presto-PR-3040 in accordance with ASTM C633 standards. The photograph of fractured surfaces of the coated specimen after pulling apart in the tensile test machine is shown in Fig. 3, where glue failure was observed. The bond strength of the coating was higher than the strength of the glue and the average breaking strength was 79.49 N/mm^2 .

3.1.4 Microstructure of the Coatings

The optical cross-sectional micrograph of the as-sprayed coating is illustrated in Fig. 4, which shows the layered



Fig. 3 Fracture surfaces of coating bond strength test

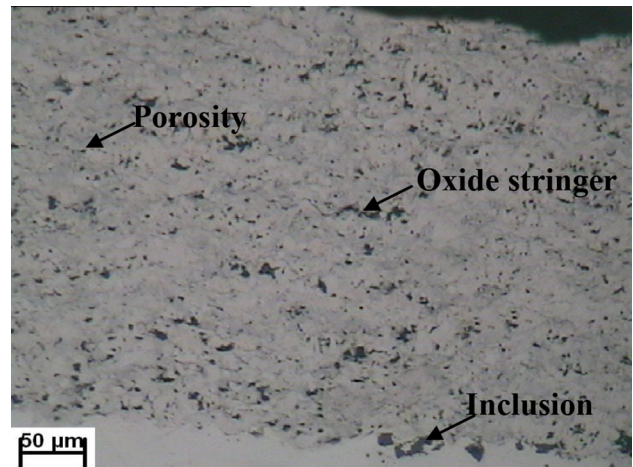


Fig. 4 Optical micrographs showing cross-sectional microstructures of as-sprayed coatings

structure of the coating built up by overlapping of molten particles, which solidifies in the form of fine splat during impact. The dark spots distributed in the optical image are the porosity. Thin contrast stringers which are oriented parallel to the substrate surface corresponds to oxides. The formation of the oxides can be attributed to the in-flight oxidation or splat surface oxidation after the impact of the powder particles. Contrast dark areas close to coating substrate interface are the inclusions. It is observed from BSEI (Fig. 5) that the coating has a dense and isotropic structure with a lower porosity which can be probably related to the higher particle kinetic energies during HVOF spraying. The chemical composition profile of the light grey phases of the coating (points 1 and 3) shows higher amount of chromium and carbon which represents the distribution of carbides in the coating. The contrast white streaks dispersed in the coating can be recognized as NiCr. It is apparent from the observation across the coating–substrate interface that interdiffusion of elements of the coating and substrate could not be found under the existing resolution of the analysis. The morphology of coating surface (Fig. 6) indicates that the coatings are having a dense microstructure and are free from cracks. One can see melted, partially melted and pores in the coating. Partially

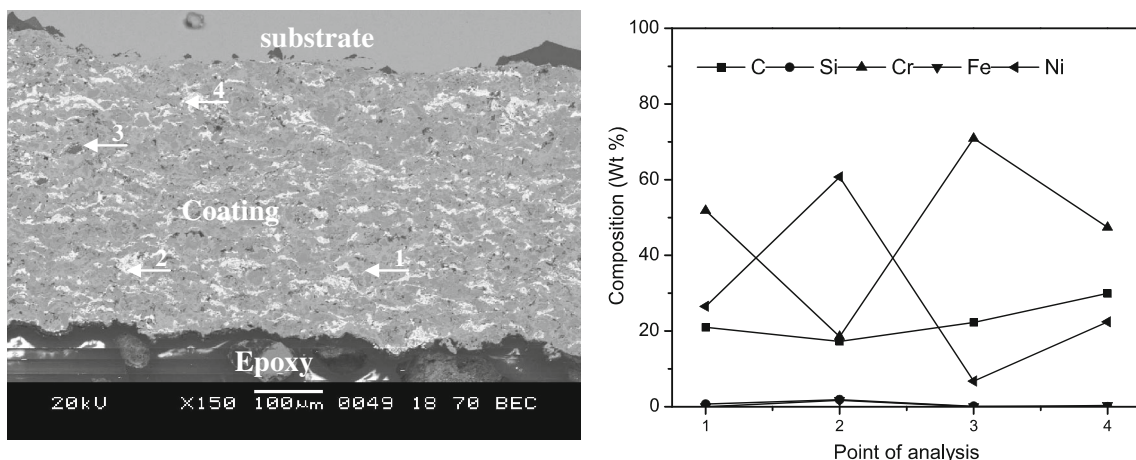
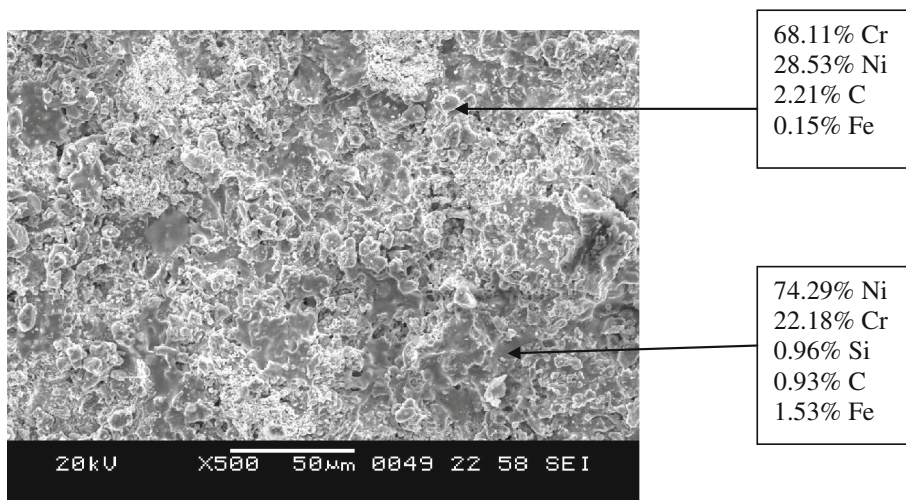


Fig. 5 BSEI and Composition profile across the cross-section of the as-sprayed coating

Fig. 6 SEM/EDAX analysis on surface of as-sprayed coating



melted areas have a composition of 68 % Cr and 28 % Ni, which is close to powder composition. Melted regions in the coating are found to be nickel-rich splats.

3.1.5 XRD Analysis of the As-sprayed Coatings

The XRD pattern for powder and as-sprayed (Cr_3C_2 -35 % NiCr) + 5 % Si coatings (Fig. 7) show that powder has major peaks of γ -Ni solid solution and Cr_3C_2 . During spraying by the HVOF process, decarburization of Cr_3C_2 might have occurred to form Cr_7C_3 phase in the coating. Formation of phases in the HVOF sprayed (Cr_3C_2 -35 % NiCr) + 5 % Si coating/powder similar to the current study were reported by Vuoristo et al. [17]. The presence of a low intensity peak of Cr_2O_3 in the as-sprayed coatings indicates that some limited oxidation of Cr occurred on the surface of in-flight particles or during solidification of impacting splats on the surface of the substrate, before the deposition of the next layer. Similar findings of formations

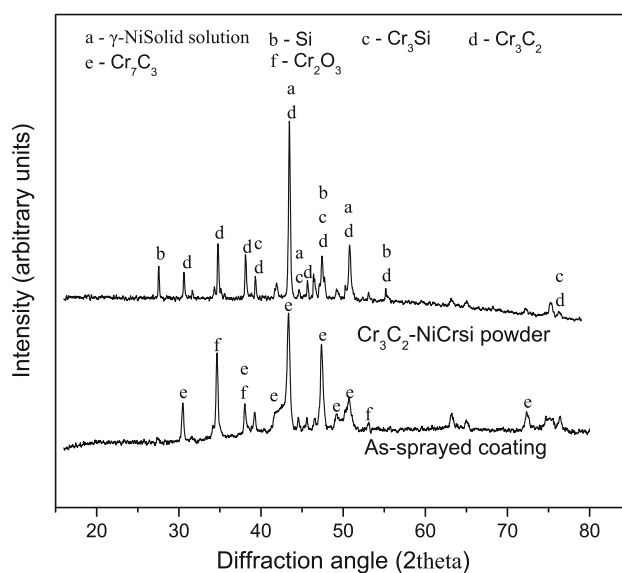


Fig. 7 XRD patterns for powder and as-sprayed coating

of oxides in the HVOF coatings have also been reported by Dent et al. [18]. The presence of Cr_3Si indicates the melting of powder during spraying to the extent of dissolution of the silicides in the liquid phase. The dissolution of Si prevents the crystallization process, evidently, a broad peak accompanied by reduction in peak intensity at 2θ of about 40° – 50° is observed for the as-sprayed coating in comparison to the initial powder. The coatings showed nearly similar peaks as compared to that of the powder representing no change in their phase composition after HVOF spraying.

3.2 Thermo Cyclic Corrosion

3.2.1 Thermogravimetry Studies

The macrographs of uncoated and coated steels subjected to hot corrosion are shown in Fig. 8. All the uncoated alloys developed a dark grey coloured oxide scale during the hot corrosion cycle. The scale formed on the uncoated T22 steel was found to be friable and showed cracks on the surface. During the initial hot corrosion cycles, spalling of oxide scale formed on the $(\text{Cr}_3\text{C}_2\text{-}35\% \text{ NiCr}) + 5\% \text{ Si}$ coated T22 steels was observed. The colour of the scale, which was dark grey during the first cycle, turned to blackish green with the progress of the study.

Subsequently, after 35th cycle, light brownish colour is observed on the surface of the sample. In the case of coated MDN steels, a dark grey colour was observed after the first cycle, which turned to blackish green during the next few cycles. The coated superfer alloy showed dark grey colour in the early cycles, which turned to brownish grey colour after 17th cycle with the indication of spalling of scale formed on the surface.

The plots of cumulative weight gain (mg/cm^2) as functions of time expressed in number of cycles are shown for uncoated and coated steels in Fig. 9a, b. The weight gain/area for the T22, MDN and Superfer steels at the end of 50 cycles are found to be 24.71, 3.97 and 3.15 mg/cm^2 , respectively. Evidently, the T22 steel showed a maximum weight gain during the hot corrosion studies in a molten salt environment as compared to the MDN and superfer steels. The total weight gain values for the coated T22, MDN and superfer steels at the end of 50 cycles of hot corrosion are found to be 7.05, 4.43 and 3.50 mg/cm^2 respectively. The coated T22 showed a higher weight gain in comparison to the other coated steels. The net weight gain for all coated steels is less compared to weight gain for uncoated steels. Therefore, it can be inferred from the thermogravimetry data that the necessary protection against hot corrosion has been provided by the $(\text{Cr}_3\text{C}_2\text{-}35\% \text{ NiCr}) + 5\% \text{ Si}$ coatings. The plot of weight gain



Fig. 8 Macrographs of uncoated substrates (*top row*, in sequence for T22, Mdn and Superfer-800H) and $(\text{Cr}_3\text{C}_2\text{-}35\% \text{ NiCr}) + 5\% \text{ Si}$ coating (*bottom row*, in sequence for T22, Mdn and Superfer—800H) subjected to hot corrosion

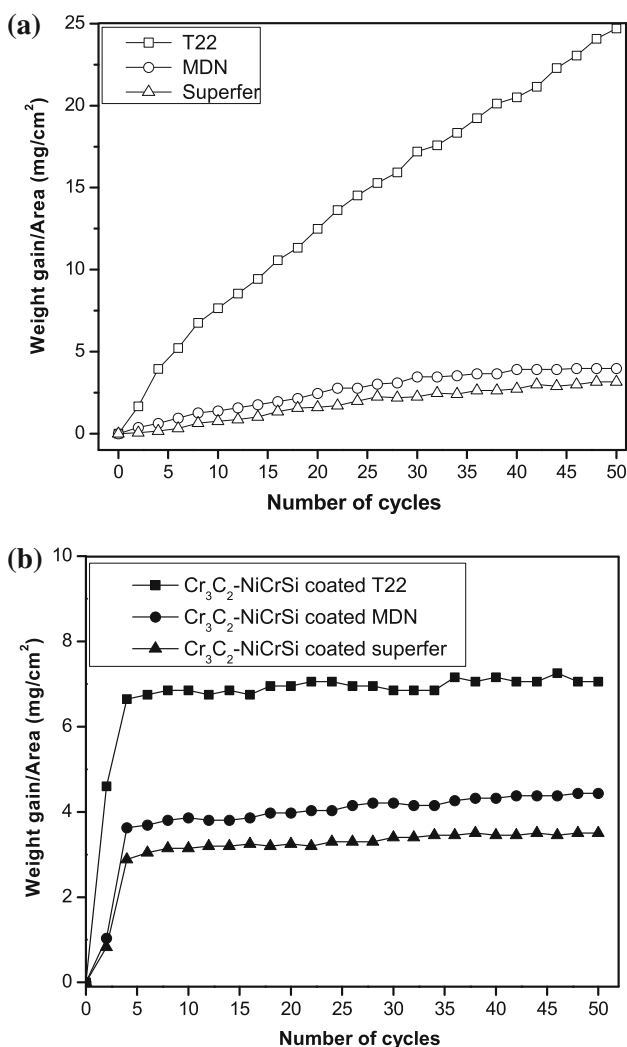


Fig. 9 Plot of weight gain/area versus number of cycles: **a** uncoated steels; **b** coated steels subjected to hot corrosion at 700 °C

square versus time (Fig. 10a) for uncoated T22 steel shows that the rate of oxidation is linear with time, which indicates that the oxide films were weakly protective at 700 °C. It is evident from the plot that the MDN and Superfer steels follow parabolic behaviour. The parabolic rate constant (K_p) was calculated by a linear least-square algorithm function in the form of $(\Delta W/A)^2 = K_p \times t$, where $(\Delta W/A)$ is the weight gain per unit area, and t is the oxidation time in seconds. The K_p for the T22, MDN and Superfer steels are 34.15×10^{-10} , 1.041×10^{-10} , $0.61415 \times 10^{-10} \text{ g}^2 \text{ cm}^{-4} \text{ s}^{-1}$ respectively. The hot corrosion behavior of the coated steels can be distinguished as a transient stage up to 4 cycles, where rapid weight gain has been observed probably due to the accelerated oxidation influenced by the molten salt environment. Thereafter, the rate of oxidation gradually reduces with time which implies the possible formation of a protective oxide scale. The slow rate of oxidation shows that the reaction rate is

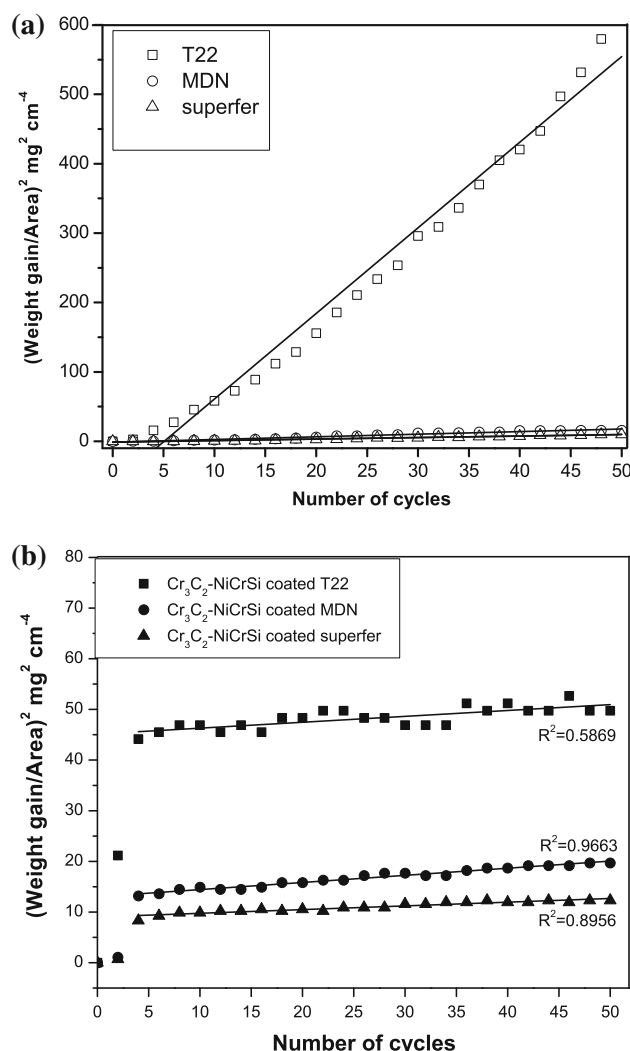


Fig. 10 Plot of $(\text{weight gain/area})^2$ versus number of cycles: **a** uncoated steels; **b** $(\text{Cr}_3\text{C}_2\text{-}35\% \text{ NiCr}) + 5\% \text{ Si}$ coated steels subjected to hot corrosion for 50 cycles at 700 °C

diffusion limited. This is substantiated from the parabolic behavior of all the coated steels as observed in Fig. 10b. The parabolic rate constants K_p for the coated T22, MDN and Superfer steels calculated from steady state region portion of the graph are 3.229×10^{-11} , 3.91×10^{-11} and $2.0 \times 10^{-11} \text{ g}^2 \text{ cm}^{-4} \text{ s}^{-1}$ respectively.

3.2.2 XRD Analysis

The XRD analysis (Fig. 11a) of hot corroded uncoated steels consisted of Fe_2O_3 as a main constituent along with Cr_2O_3 , FeS_2 and CrVO_3 . In addition, uncoated MDN and Superfer steels (Fig. 11b) showed the presence of NiO and NiVO_3 in the oxide scale. The XRD analysis of the $(\text{Cr}_3\text{C}_2\text{-}35\% \text{ NiCr}) + 5\% \text{ Si}$ coated steels (Fig. 12a, b) subjected to hot corrosion, reveals the formation of the major phases like Cr_2O_3 , NiCr_2O_4 and Ni_2SiO_4 . During spraying of the

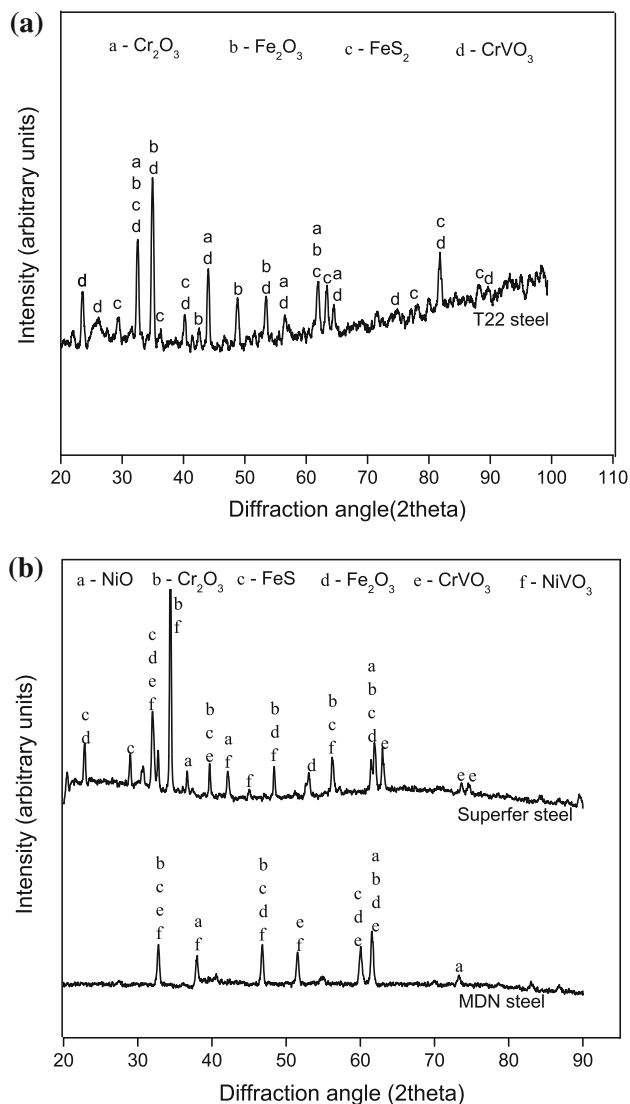


Fig. 11 XRD patterns for uncoated steels subjected to hot corrosion in Na_2SO_4 -60 % V_2O_5 for 50 cycles at 700 °C: **a** T22 steel; **b** MDN and superfer steel

HVOF process, decarburization of Cr_3C_2 might have occurred to form Cr_7C_3 phase, subsequently Cr_{23}C_6 and Cr_2O_3 phase in the coating.

3.2.3 SEM/EDAX Analysis

The SEM micrograph showing the surface scale morphology along with EDAX analysis at some selected sites of interest on the coated steels in the molten salt environment at 700 °C are shown in Fig. 13. The surface scale developed on coated steels is massive, crackfree with dense clusters mainly consisting of Cr_2O_3 , NiO and V_2O_5 . The oxide scale on coated T22 steel (Fig. 13a) has a blade-like structure with smooth patches. The EDAX analysis on these patches (point 1) indicates a higher percent of Cr_2O_3

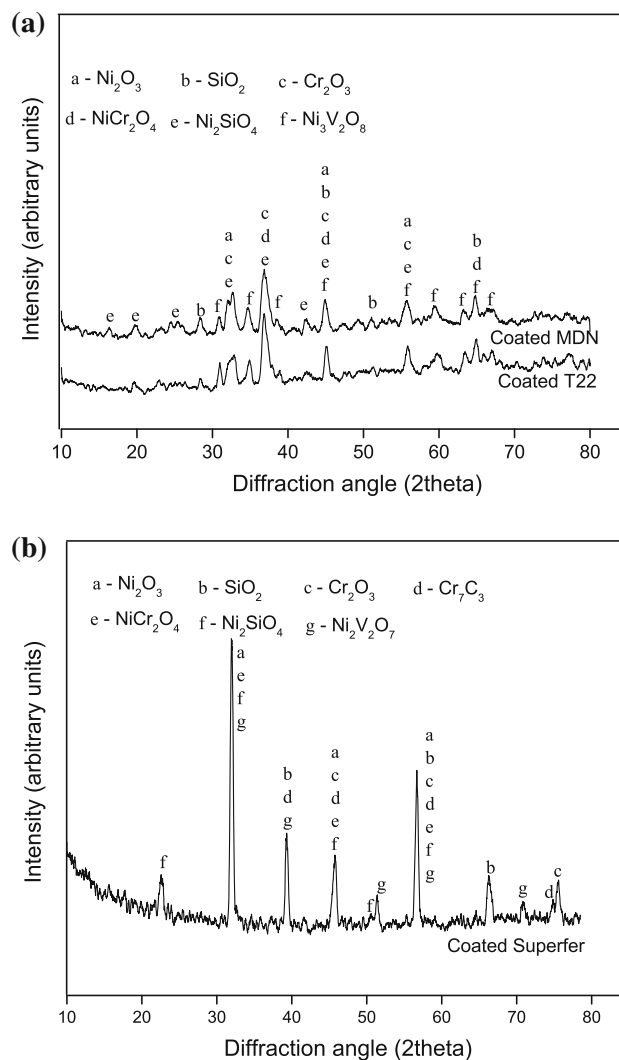


Fig. 12 XRD patterns for coated steels subjected to Hot corrosion: **a** T22 and MDN steels; **b** superfer steels

and V_2O_5 in contrast globules (point 2) has higher amount of Cr_2O_3 , NiO and V_2O_5 . Superfer coated steel (Fig. 13b) reveal 39.32 % Cr_2O_3 , 21.31 % NiO and 21.40 % V_2O_5 (at Point 1) and 30.88 % NiO, 36.52 % V_2O_5 and 10.46 % SiO_2 (at Point 2) along with small quantities of C, Na_2O and SO_3 .

3.2.4 Cross-sectional Analysis

BSEI and elemental variation across the cross-section of hot corroded (Cr_3C_2 -35 % NiCr) + 5 % Si coated Superfer steel in molten salt environment at 700 °C are shown in Fig. 14. A continuous, lamellar, crack free and uniform oxide scale forms on the coated steel which has retained the dense structure of the as sprayed coatings even after the hot corrosion run for 50 cycles. The topmost part of the scale (point 1 and 2), containing mainly Cr and Ni with about 20

Fig. 13 Surface scale morphology and EDAX point analysis for coated steels subjected to hot corrosion: **a** T22 steel; **b** Superfer steel

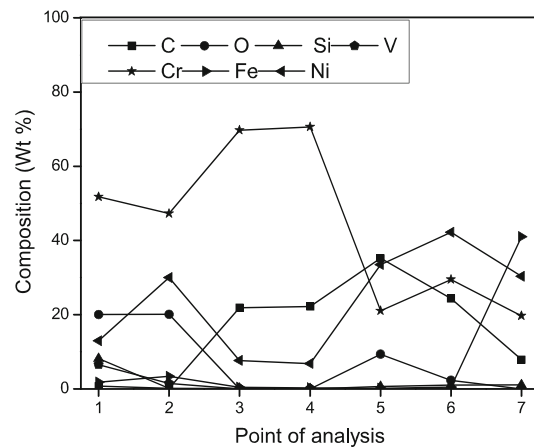
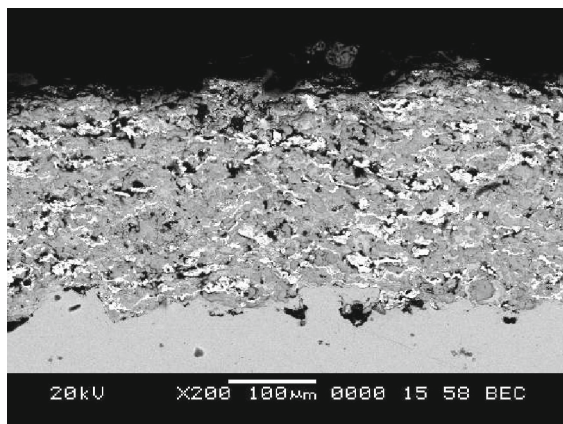
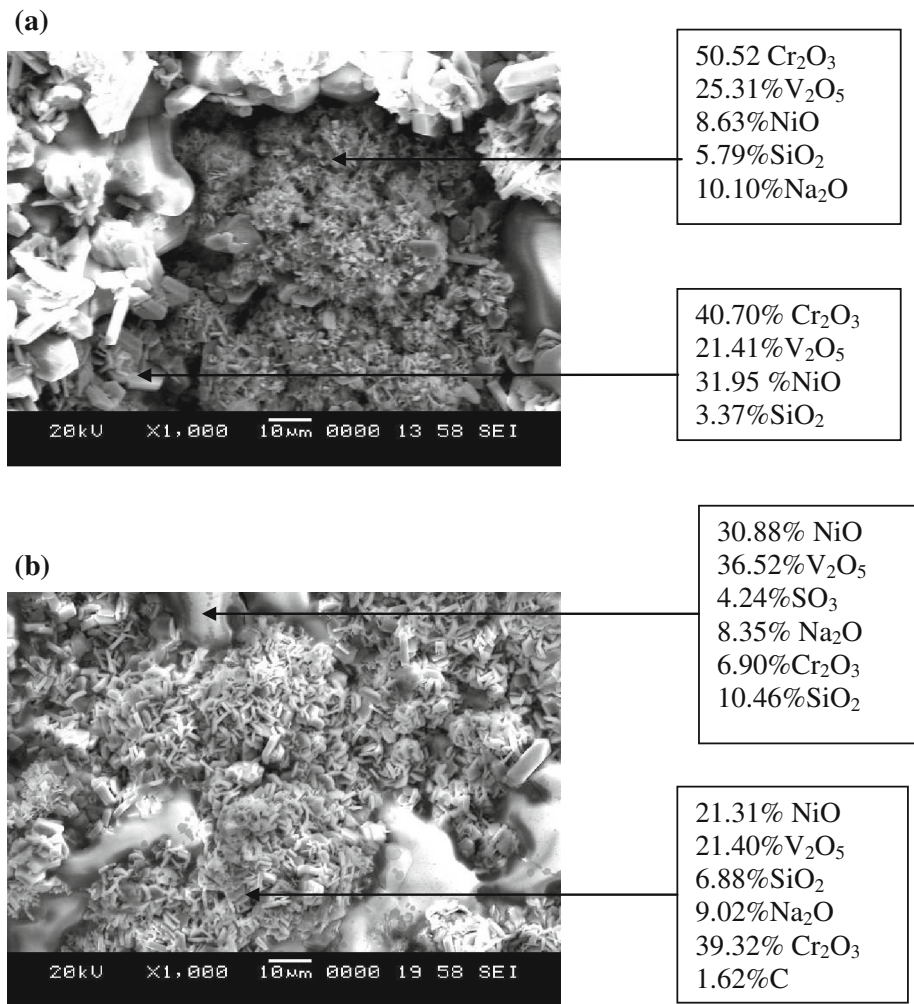
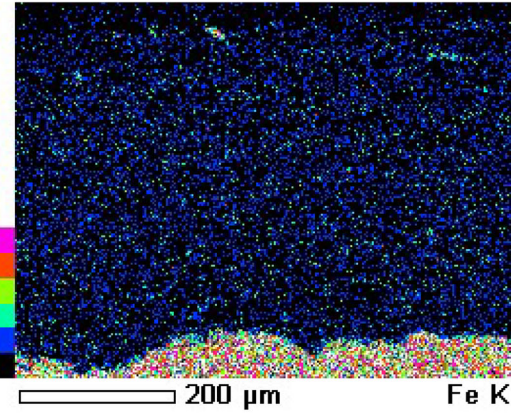
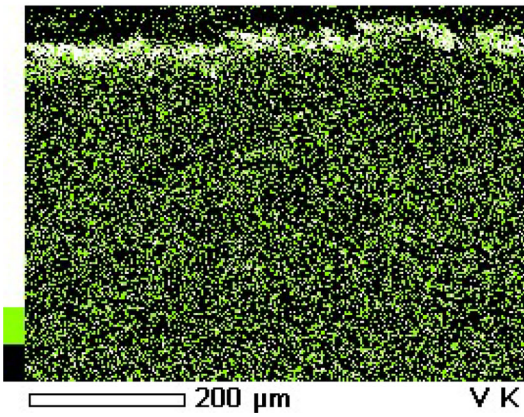
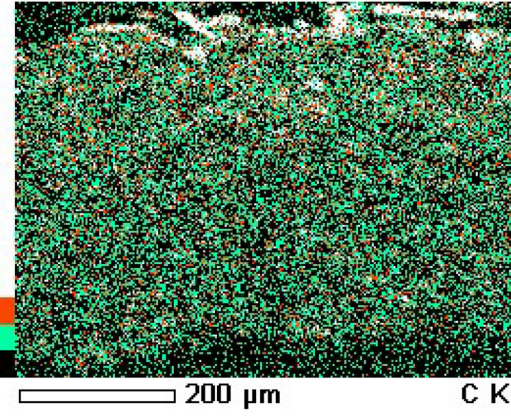
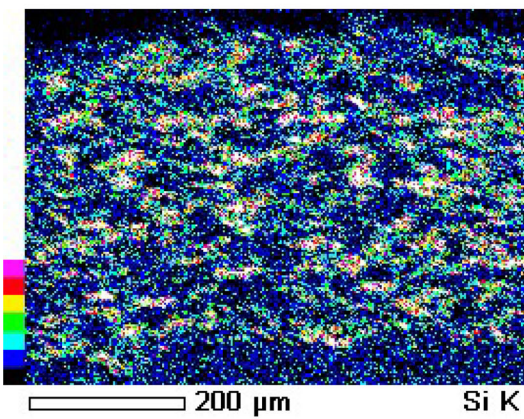
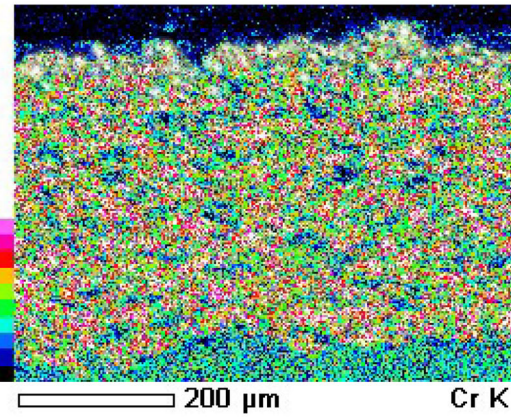
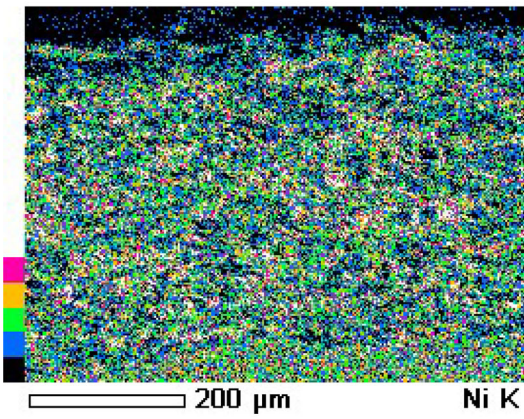
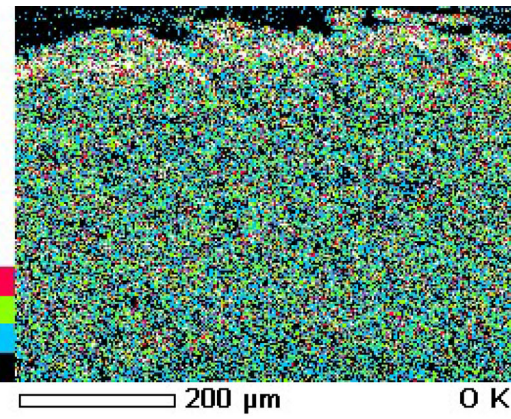
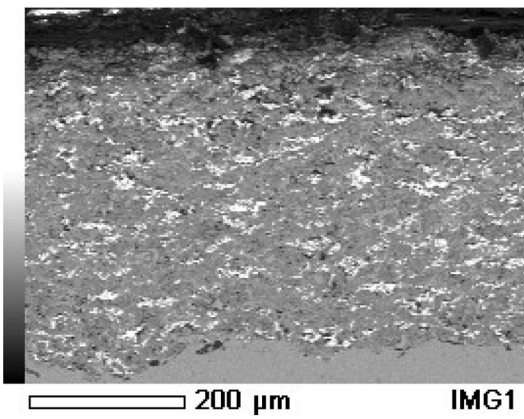


Fig. 14 Back scattered electron image and EDAX point analysis (wt%) across the cross-section of the (Cr₃C₂-35 % NiCr) + 5 % Si coated superfer steels subjected to hot corrosion

wt% of O is rich in oxides of Ni and Cr and their spinels. The splat boundaries (points 5 and 6) in the scale are detected as nickel and chromium rich splats, mostly in a un-oxidised state, as the relatively lesser amount of oxygen

is present at these points. A minor amount of oxides in these splat boundaries are believed to be formed as a result of in-flight oxidation of NiCr powder during deposition. The coating splats (points 3 and 4) consist mainly of



◀ **Fig. 15** BSEI and elemental X-ray mapping at the cross-section of the $(\text{Cr}_3\text{C}_2\text{-}35\% \text{ NiCr}) + 5\% \text{ Si}$ coated Superfer steels subjected to hot corrosion

chromium and carbon with a significant decrease in nickel. The absence of oxygen at these points as well as at the coating–substrate interface indicates that the oxidation is restricted only to the surface of the coating and the surface oxide scale acts as a diffusion barrier to the penetration of oxidizing species.

3.2.5 Elemental X-ray Mapping

Figure 15 shows the elemental X-ray mapping for the $(\text{Cr}_3\text{C}_2\text{-}35\% \text{ NiCr}) + 5\% \text{ Si}$ coated superfer steel after its exposure to the molten salt environment for 50 cycles at 700 °C. Elemental mapping for Cr, Ni, Si and O showed that the oxide scale formed on the surface contains Cr_2O_3 , SiO_2 and NiO and their spinel oxides of NiCr_2O_4 and Ni_2SiO_4 . The coating is oxidized partially which is mainly restricted to the surface. The combined mapping for Cr and C reveals thin stringers of Chromium carbide on the oxide scale. The presence of Ni, V and O at the upper part of the scale indicates the formation of $\text{Ni}_2\text{V}_2\text{O}_7$ spinel on the top surface. The higher concentration of vanadium is confined only to the surface and not penetrated much into the coating during the hot corrosion cycles. Hence the oxide scale formed seems to be effective in preventing the transport of corrosive species into the surface. Closer look into Ni and Fe maps indicate the interdiffusion of Ni from the coating into the substrate as well as diffusion of Fe from the substrate into the coating. It is very interesting to note that the concentration of Cr remains the same throughout the scale and its concentration did not get reduced by diffusion.

4 Discussion

The desirable thicknesses of the coatings in the range of 350–400 μm have been successfully deposited on the substrate alloys. Heath et al. [19] has reported that the thick coatings have better corrosion resistance. The lower value of porosity of the coatings is related to higher kinetic energies of powder particles and to the melting behavior exhibited by the particles during HVOF spraying. The partially melted particles form an almost porosity-free coating when they reach the substrate at high velocity. The measured values of the porosities are in good agreement with the findings of Sahraoui et al. [20] for the HVOF sprayed $\text{Cr}_3\text{C}_2\text{-}25\% \text{ NiCr}$ coatings. The coatings have retained the phases observed in starting powder and do not undergone significant phase transformation.

The weight gain of the coated specimens is relatively high during the initial four cycles of hot corrosion, but subsequently increase in weight gain is gradual. The higher weight gain of the specimens during the first few cycles might be due to the formation of oxides of each and every active element present in the coating. Thereafter, the oxidation rate drops drastically due to the formation of protective oxide scale of Cr_2O_3 and SiO_2 that restricts the diffusion of O_2 or other corrosive elements through it. The slow rate of oxidation shows that the reaction rate is diffusion limited. The chromium exhibits higher affinity for oxygen to form Cr_2O_3 during the early stages of hot corrosion which lowers the oxygen potential, promoting the lateral growth of SiO_2 and NiO rather than nucleation. Choi et al. [21] reported similar observation for the plasma sprayed NiCrAlY coatings on Nimonic 80A and SS41 alloy substrates. Subsequent to more stable binary oxides formed on the surface, ternary oxides (NiCr_2O_4 and Ni_2SiO_4) have formed during the intermediate stages of hot corrosion. The presence of the spinel NiCr_2O_4 and Ni_2SiO_4 in the oxide scales improves the oxidation resistance in the molten salt environment as these spinel phases usually have much smaller diffusion coefficients for the cations and anions than those in their parent oxides as reported by Chatterjee et al. [22].

The X-ray mapping and EDAX analysis along the cross section shows the distribution of Vanadium on the uppermost oxide scale and hence, the acidic fluxing by $\text{Na}_2\text{SO}_4\text{-}60\% \text{ V}_2\text{O}_5$ mixture is expected. Based on the available thermodynamic data, Na_2SO_4 can react with V_2O_5 to increase the acidity of melt by the formation of vanadates. The vanadates act as a catalyst, resulting in the acidic dissolution of metal oxides to form metal vanadates which are concentrated mainly in the top scale.

SiO_2 appears to have a better corrosion resistance in the given environment and in the highly acidic melts, SiO_2 scales has the minimal solubility. Furthermore, silicon and vanadium apparently do not form any compounds with each other. Nicoll [23] opined that the modification of standard MCrAlY coating systems with Si additions of up to 2.7 % leads to an improvement in both oxidation and corrosion resistance. Grunling and Bauer [24] reported that SiO_2 affords a better protection than that of Cr_2O_3 which is susceptible to vaporization loss by forming CrO_3 at a temperature of about 1,000 °C.

It is evident from Figs. 14 and 15 that the coatings have been partially oxidized and the corrosion is restricted to a depth of a few microns on the surface at the end of 50 cycles of hot corrosion cycles. The absence of oxygen as well as Na and V is observed in the region below the surface oxide layer. The surface scale acts as a barrier to the diffusion of O_2 and the corrosive species of the molten salt into the inside of the coating, thereby, contributing to

the hot corrosion resistance of coatings. This can be further substantiated from the weight gain square (mg^2/cm^4) data plotted as a function of time (Fig. 10b), which shows a parabolic behaviour of all the coated steels. The coated steels showed a lower weight gain in comparison to the uncoated steels.

The coefficients of thermal expansion of SiO_2 , Cr_2O_3 and NiO are in close range and, hence, the thermal stresses are minimized. The oxide scale formed on the coated steels appears to be adherent and dense without any scale spalling or cracking. The oxides formed are effective in protecting the substrate alloys, as the cycle-oxidation behaviour of an alloy is dictated mainly by the scale spallation resistance [25].

Differences in chemical compositions between a coating and substrate alloys can lead to inter-diffusion between these materials which can alter high temperature corrosion resistance of the coating. Shifler [26] reported that high-temperature coatings on various substrate steels behaved differently in molten salt environment at 899°C . The relative hot corrosion resistance of the $(\text{Cr}_3\text{C}_2\text{-}35\% \text{ NiCr}) + 5\% \text{ Si}$ coated steels based on the thermogravimetric data, can be arranged in the order: Superfer 800H > MDN 310 > T22.

5 Conclusions

- High velocity oxy-fuel thermal spraying with oxygen and liquid petroleum gas as the fuel gas has been used successfully to deposit $(\text{Cr}_3\text{C}_2\text{-}35\% \text{ NiCr}) + 5\% \text{ Si}$ alloy coatings on three kinds of substrate steels. Seemingly dense laminar structured coating with porosity less than 1.5 % and average microhardness of 736 HV have been achieved. The bond strength of the coating is higher than 80 N/mm^2 .
- The coatings exhibit almost similar peaks as compared to that of the powder, indicating no change in their phase composition after spraying. The powder and as-sprayed coating have major phases of $\gamma\text{-Ni}$ solid solution and Cr_3C_2 .
- The superior corrosion resistance of the coated steels, in the presence of the highly acidic molten salt can be ascribed to continuous and protective oxide scale of Cr_2O_3 and SiO_2 which restricts the diffusion of O_2 or other corrosive elements through it. The coating region underneath the uppermost oxide scale remains unoxidised.
- The corrosion kinetics of the coated steels showed parabolic behaviour and the parabolic rate constant values are significantly lower in comparison to the uncoated steels. The oxide scale formed on the corroded coatings seems to be compact and adherent demonstrating resistance to scale spalling.

- The coating has provided the higher hot corrosion resistance to Superfer 800H followed by MDN 310 and T22 steels. The parabolic rate constant for the coated T22 is much higher as a result of spalling of oxide scale formed on the surface of coatings.

Acknowledgments The authors gratefully acknowledge M/S Metallizing Equipment Co. Pvt. Ltd., Jodhpur, India for having provided coating facility and MIDHANI Hyderabad for supplying the substrate steels. They also wish to acknowledge National Institute of Technology, Surathkal and Poornaprajna Institute of Scientific Research (PPISR), Bengaluru for providing SEM/EDAX and XRD facilities.

References

- Natesan K, *Surf and Coat Technol* **56** (1993) 185.
- Harb J N, and Smith E E, *Energy Combust Sci* **16** (1990) 169.
- Uusitalo M A, Vuoristo P M J, and Mantyla T A, *Mater Sci Eng A-Struct* **346** (2003) 168.
- Hidalgo H V, Belzunce Varela J, Carriles Menéndez A, and Poveda Martínez S, *Wear* **247** (2001) 214.
- Gurrappa I, *Mater Sci and Technol* **19** (2003) 178.
- Parker D W, and Kutner G L, *Adv Mater Proc* **139** (1991) 68.
- Li C-J, Wang Y-Y, and Li H, *J Vac Sci Technol A* **22** (2004) 2000.
- Guilemany J M, Miguel J M, Vizcaino S, Lorenzana C, Delgado J, and Sanchez J, *Surf Coat Technol* **157** (2002) 207.
- Seong B G, Hwang S Y, and Kim K Y, *Surf Coat Technol* **126** (2000) 256.
- Toma D, Brandl W, and Marginean G, *Surf Coat Technol* **138** (2001) 149.
- Sidhu T S, Prakash S, and Agrawal R D, *J Thermal Spray Technol* **15** (2006) 387.
- Gurrappa I, *Surf and Coat Technol* **139** (2001) 272.
- Ramesh M R, Prakash S, Nath S K, Sapra P K, and Krishnamurthy N, *J Thermal Spray Technol* **20** (2011) 992.
- Wu Y, and Niu Y, *Scr Mater* **53** (2005) 1247.
- Zeng Z, Kuroda S, Kawakita J, Komatsu M, and Era H, *J Thermal Spray Technol* **19** (2010) 128.
- Sundararajan T, Kuroda S, and Abe F, *Mater Trans* **45** (2004) 1299.
- Vuoristo P, Niemi K, Makela A, and Mantyla T, in Proc of the 7th National Thermal Spray Conference on *Abrasion and Erosion Wear Resistance of $\text{Cr}_3\text{C}_2\text{-NiCr}$ Coatings Prepared by Plasma, Detonation and High-Velocity Oxyfuel Spraying*, Boston, Massachusetts, (1994), p 121.
- Dent A H, Horlock A J, McCartney D G, and Harris S J, *Surf and Coat Technol* **139** (2001) 244.
- Heath G R, Heimgartner P, Irons G, Miller R, and Gustafson S, *Mater Sci Forum* **251–254** (1997) 809.
- Sahraoui T, Fenineche T-E, Montavon G, and Coddet C, *Mater Des* **24** (2003) 309.
- Choi H, Yoon B, Kim H, and Lee C, *Surf Coat Technol* **150** (2002) 297.
- Chatterjee U K, Bose S K, and Roy S K, *Environmental Degradation of Metals*, Marcel Dekker Publications, New York (2001).
- Nicoll A R, *Thin Solid Films* **95** (1982) 285.
- Grunling H W, and Bauer R, *Thin Solid Films* **95** (1982) 3.
- Stott F H, *Mater Charact* **28** (1992) 311.
- Shifler D A, in Proc of 5th International Symposium on *High Temperature Corrosion and Materials Chemistry*, Electrochemical Society, vol. 16 (2004), p 295.